Korean J. of Chem. Eng., **5**(1) (1988) *60-66*

A NUMERICAL AND EXPERIMENTAL STUDY OF FLUID FLOW IN CONTINUOUS CASTING MOLD

Sung Woo LEE and Moon Ho SUH*

Continuous Casting Lab., Research Institute of Industrial Science & Technology, Pohang 790-330, Korea
*Department of Chemical Engineering, Ajou University, Suwon 440-749, Korea
(Received 18 May 1987 • accepted 23 September 1987)

Abstract—To study removal of nonmetallic inclusion in continuous casting mold, both flow visualized experiments and computer simulations were carried out using a 1/2 scale water model of the mold. The effect of port angle of submerged nozzle on the floatability of nonmetallic inclusion was also examined.

The velocity fields predicted by solving the turbulent Navier-Stokes equations using the K-ε model for turbulent viscosity were found to be in good qualitative agreement with the results of water model experiments. The result of the present work could be used to predict the characteristics of fluid flow in a continuous casting mold.

INTRODUCTION

Flow behavior of molten steel in the continuous casting process has important implications with regard to both the quality control of the final products and the ease of operation. Especially, the mold system of continuous casting is called upon to perform two vital functions. These are separation of nonmetallic inclusions and solidification of the distributed hot metal between strands.

Unlike ingot casting, little time is available for the separation of nonmetallic inclusions in the continuous casting mold system. Thus, fluid flow parameters must be controlled to maximize the available separation time and minimize the influx and production of nonmetallics.

The nonmetallic inclusions are transported to the mold by way of the flow stream in which the inclusions are entrained, and removal of inclusion is accomplished by one or both of the following mechanisms:

(1) direct interaction of inclusions with steel/slag interface and removal into the slag or attachment to the refractories

(2) floatation of relatively large inclusions from the metal stream

The removal of nonmetallic inclusion is promoted by the following methods:

(1) vortex prevention
(2) maximization of the minimum residence time
(3) minimization of dead volume
(4) control of mixed and plug flow regions

Since the removal of nonmetallic inclusion is strongly related to the flow behavior of molten steel in the tundish and/or mold, the flow field analysis has been the subject of a large number of theoretical and experimental investigations [1–4]. However, the majority of previous investigations were restricted to the tundish system. In the present study, we extended the flow field analysis to the mold system and the effect of port angle of submerged nozzle on the removal of nonmetallic inclusion was also examined.

THEORETICAL ANALYSIS

Flow volumes in the mold

To facilitate the study of mixing conditions in a mold system, two idealized patterns of flow have been accepted by investigators in this field. The term "back-mixing flow" is used to describe complete and instantaneous mixing in the system. On the other hand, "plug flow" assumes that a fluid element moves through the system without overtaking or mixing with fluid entering at an earlier or later time. In addition to the two idealized patterns of flow, dead flow accounts for the portion of fluid which is moving so slowly that it may be assumed to be stagnant.

The flow patterns in a real mold may be approximated by a combination of the above flows, as shown in Figure 1. The mold is assumed to be consisted of interconnected flow regions with various modes of flow existing between them. The flow pattern may be determined directly from the flow paths of fluid through the mold. However, the difficulty of obtaining and inter-

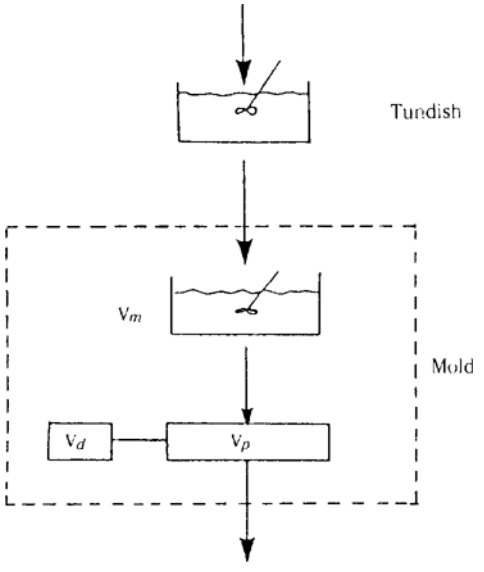

Fig. 1. Representation of flow volumes in the mold system.

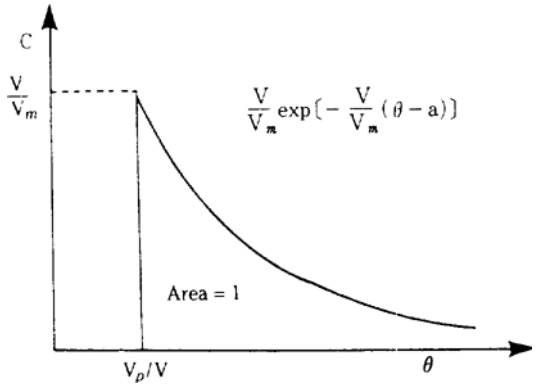

Fig. 2. Multiparameter model and its response curve.

preting such information has led to the alternate approach of determining the RTD (Residence Time Distribution) of fluid elements by means of stimulus-response studies. The stimulus is provided by introducing a tracer in the inlet stream and recording the changes in tracer concentration in the exit stream.

As illustrated in Figure 1, the model assumes that the volume in the mold can be divided into the three separate flow regions. The proportions of the total volume that are backmix flow, plug flow and dead volume can be determined from the peak concentration on the RTD curves, respectively. The characteristic features of the model are [5, 6]:

$$V_d / V = 1 - \theta_{av} \tag{1}$$

$$V_p / V = \theta_{peak} \tag{2}$$

$$V_m / V = 1 / C_{max} \tag{3}$$

$$V_d + V_p - V_m = V \tag{4}$$

The vertical rise of tracer concentration at time θ_{peak} as shown in Figure 2 is a reflection of the existence of a plug volume, where diffusion or mixing of tracer is absent.

Mathematical modeling of the mold

For the computation of fluid flow in the mold certain assumptions are made to ease the complexity of the task. First, since the velocity variation along the thickness of the mold is substantially lower in comparison with the corresponding variation along the other two directions, the velocity field is presented in two directions along the width and the depth of the molten steel.

Secondly, the flow is assumed to be isothermal, incompressible, and steady. The assumption of steady state, i.e., that the liquid metal holdup in the mold does not change with time, is made for simplicity. Furthermore, the thickness of the slag layer is considered to be small, and it is assumed that the existence of a slag layer does not influence to the fluid flow field in the metal phase significantly.

The equations used in fluid flow predictions are the equation of continuity and the equation of momentum in two dimensions.

Equation of continuity

$$\frac{\partial}{\partial x_i}(\rho u_i) = 0 \tag{5}$$

Equation of momentum

$$\frac{\partial}{\partial x_i}(\rho u_i u_j) = -\frac{\partial P}{\partial x_j} + \frac{\partial}{\partial x_i}\left[\mu_e\left(\frac{\partial u_j}{\partial x_i} + \frac{\partial u_i}{\partial x_j}\right)\right] \tag{6}$$

The effective viscosity, μ_e, is considered to be composed of the molecular and turbulent components.

$$\mu_e = \mu + \mu_t \tag{7}$$

And the turbulent viscosity, μ_t, was calculated by the K-ε model of turbulence as the following:

$$\mu_t = C_D \rho K^2 / \varepsilon \tag{8}$$

The K-ε model of Launder and Spalding [7] entails the solution of two differential equations for the kinetic energy of turbulence (K) and the turbulence energy dissipation rate (ε). Governing transport equations for K and ε can be represented as follows:

$$\frac{\partial}{\partial x_i}\left(\rho u_i K - \frac{\mu_e}{\sigma_k}\frac{\partial K}{\partial x_i}\right) = G - \rho\varepsilon \tag{9}$$

$$\frac{\partial}{\partial x_i}\left(\rho u_i \varepsilon - \frac{\mu_e}{\sigma_\varepsilon}\frac{\partial \varepsilon}{\partial x_i}\right) = (C_1 G - C_2 \rho \varepsilon)\varepsilon / K \tag{10}$$

Table 1. Values of constants in K-ε turbulence model.

C_1	C_2	σ_k	σ_ε	C_D
1.43	1.92	1.00	1.30	0.09

$$\text{where, } G=\mu_t\frac{\partial u_i}{\partial x_i}\left(\frac{\partial u_j}{\partial x_i}+\frac{\partial u_i}{\partial x_j}\right) \tag{11}$$

Knowledge of K and ε allows the length scale to be determined and also the effective viscosity from which the turbulent shear stress can be calculated.

For the computational purpose the following stream function and vorticity were introduced.

$$u_x=\frac{\partial \psi}{\partial y},\quad u_y=-\frac{\partial \psi}{\partial x} \tag{12}$$

$$\xi=-\left(\frac{\partial^2\psi}{\partial x^2}+\frac{\partial^2\psi}{\partial y^2}\right) \tag{13}$$

Then vorticity transport equation can be easily derived by partial differentiation and manipulation of the momentum equations.

$$\rho\left\{\frac{\partial}{\partial x}\left(\xi\frac{\partial\psi}{\partial y}\right)-\frac{\partial}{\partial y}\left(\xi\frac{\partial\psi}{\partial x}\right)\right\}$$

$$=\frac{\partial}{\partial x}\left\{\frac{\partial}{\partial x}(\mu_e\xi)\right\}+\frac{\partial}{\partial y}\left\{\frac{\partial}{\partial y}(\mu_e\xi)\right\} \tag{14}$$

In order to determine the eddy viscosity for turbulence, K and ε were calculated by solving the following equations.

$$\rho\left\{\frac{\partial}{\partial x}\left(K\frac{\partial\psi}{\partial y}\right)-\frac{\partial}{\partial y}\left(K\frac{\partial\psi}{\partial x}\right)\right\}$$

$$=\left\{\frac{\partial}{\partial K}\left(\frac{\mu_e}{\sigma_k}\frac{\partial K}{\partial x}\right)+\frac{\partial}{\partial y}\left(\frac{\mu_e}{\sigma_k}\frac{\partial K}{\partial y}\right)\right\}+S_k \tag{15}$$

$$\rho\left\{\frac{\partial}{\partial x}\left(\varepsilon\frac{\partial\psi}{\partial y}\right)-\frac{\partial}{\partial y}\left(\varepsilon\frac{\partial\psi}{\partial x}\right)\right\}$$

$$=\left\{\frac{\partial}{\partial\varepsilon}\left(\frac{\mu_e}{\sigma_\varepsilon}\frac{\partial\varepsilon}{\partial x}\right)+\frac{\partial}{\partial y}\left(\frac{\mu_e}{\sigma_\varepsilon}\frac{\partial\varepsilon}{\partial y}\right)\right\}+S_\varepsilon \tag{16}$$

where
$$S_k=G-\rho\varepsilon \tag{17}$$

$$S_\varepsilon=C_1\varepsilon G/K-C_2\rho\varepsilon^2/K \tag{18}$$

$$G=\mu_t\left[2\left\{\left(\frac{\partial u_x}{\partial x}\right)^2+\left(\frac{\partial u_y}{\partial y}\right)^2\right\}+\left(\frac{\partial u_x}{\partial y}+\frac{\partial u_y}{\partial x}\right)^2\right] \tag{19}$$

According to the recommendation of Launder and Spalding [7], the five constants appearing in the above equations take the values given in Table 1.

The boundary conditions used for the numerical solution of the above set of partial differential equations are:

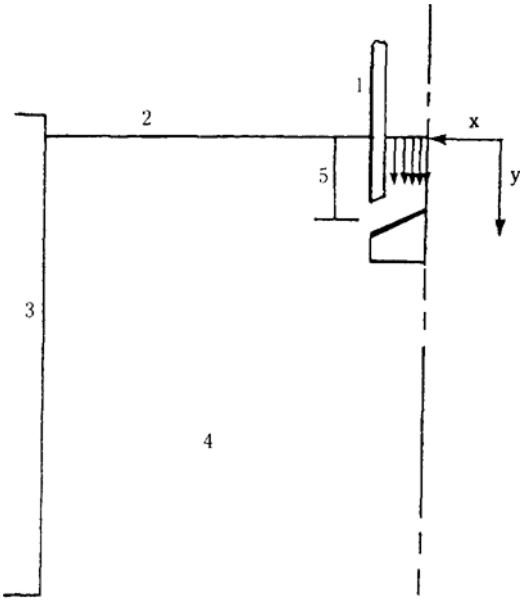

1. Submerged nozzle 2. Meniscus
3. Mold wall 4. Molten steel
5. Immersion depth

Fig. 3. Schematic sketch of the mold system showing one half of the mold.

at the axis of symmetry,

$$\psi=\text{constant},\quad \frac{\partial\xi}{\partial x}=\frac{\partial K}{\partial x}=\frac{\partial\varepsilon}{\partial x}=0$$

at the free surface,

$$\xi=\text{constant},\quad \frac{\partial K}{\partial y}=\frac{\partial\varepsilon}{\partial y}=0$$

at the walls,

$$\psi=0,\quad K=\varepsilon=0$$

Close to the side walls, the variation in flow properties are much steeper than within the bulk fluid. Consequently, velocity components (u_x, u_y) and scalar transport properties (K, ε) were determined by using wall functions.

Numerical simulation procedure

The governing equations were solved numerically using a semi-implicit upwind difference scheme [8, 9] over the flow domain shown in Figure 3.

Prior to the application of the numerical scheme for the calculations reported in this paper, the scheme was examined for accuracy. The computer program was used to simulate simple laminar flow in a pipe for which an analytical solution of the governing equations is available. And excellent agreement was achieved between the numerical predictions and the analytical results, as shown in Figure 4.

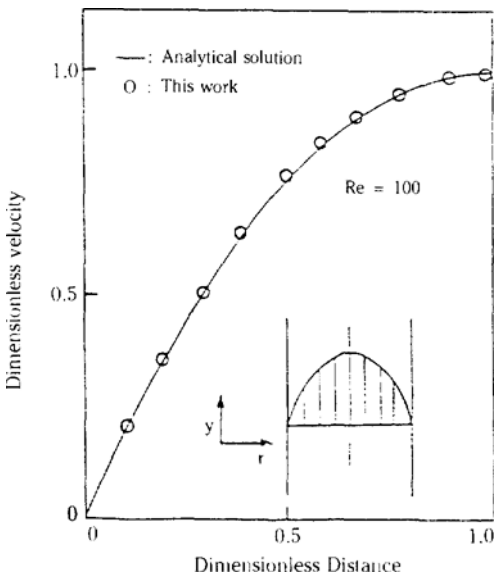

Fig. 4. Velocity distribution for Poiseuille flow.

Table 2. Physical properties of water and molten steel.

Physical properties	Water at 20°C	Molten steel at 1600°C
Viscosity, cp	1.0	6.4
Density, kg/m^3	1,000	7,014
Kinematic viscosity, cs	1.0	0.913
Surface tension, dyne/cm	73.05	1,600

The computer time required in the simulation of the mold system were of the order of 50 minutes on the PRIME 750 digital computer and CALCOMP 965 Plotter. Computations were carried out until the absolute sum of normalized residuals for u_x, u_y, K, ε and continuity should be converged to 10^{-3}.

WATER MODEL EXPERIMENTS

In the investigation of the flow of molten steel, water is often used as a modeling fluid because it is easy to obtain, easily handled, and its kinematic viscosity is comparable to that of molten steel. The physical properties of water at 20°C and molten steel at 1600°C are compared in Table 2.

Using water as a modeling fluid for molten steel, it is impossible to satisfy all three of the dimensionless governing numbers simultaneously [10]. While Reynolds and Froude numbers may be concurrently satisfied with a full scale model, a model of 1/2 scale is needed to satisfy the Weber and Froude numbers concurrently.

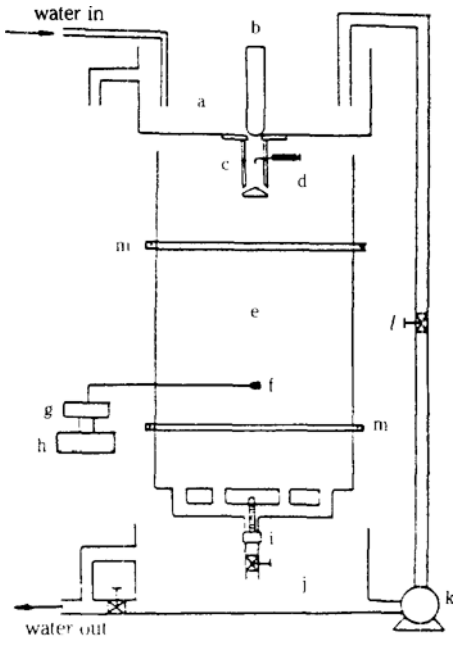

a. Tundish
b. Stopper
c. Submerged nozzle
d. Injection port
e. Mold
f. Pt-wire sensor
g. Amplifier
h. Recorder
i. Flowmeter
j. Water reservoir
k. Pump
l. Valve
m. Support

Fig. 5. Schematic diagram of water model apparatus.

Table 3. Physical parameters in full-scale and experimental model for the mold system.

Physical parameters	Full-scale	1/2 water model
Casting speed, m/min	1.2	0.96
Fluid	steel	water
Mold size (W × T × L), m	1.6 × 0.22 × 0.9	0.8 × 0.11 × 1.5
Submerged depth of nozzle, m	0.1—0.2	0.1
Total flow rate, l/min	422.4	84.6

Experimental work for the mold system were carried out in a 1/2 scale water model of the actual mold and a schematic diagram of the apparatus is shown in Figure 5. Principal dimensions of the mold, together with operating parameters, are summarized in Table 3. The mold models were fabricated from clear acrylic sheet and flow visualization is facilitated by introduc-

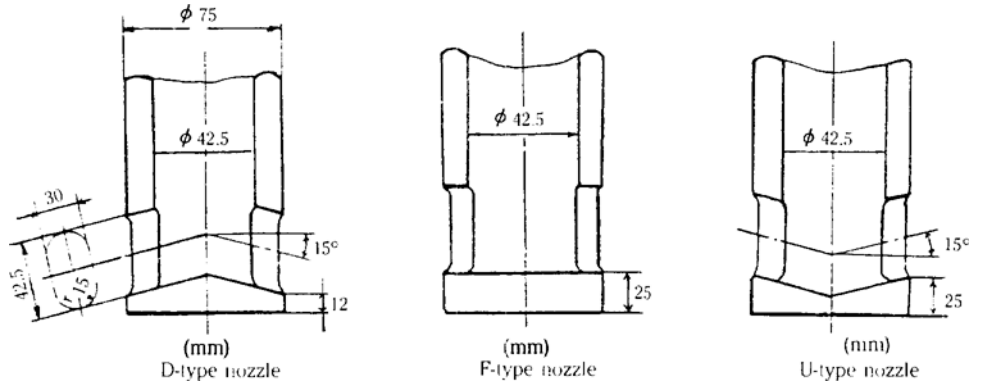

Fig. 6. Types and dimensions of the submerged nozzles.

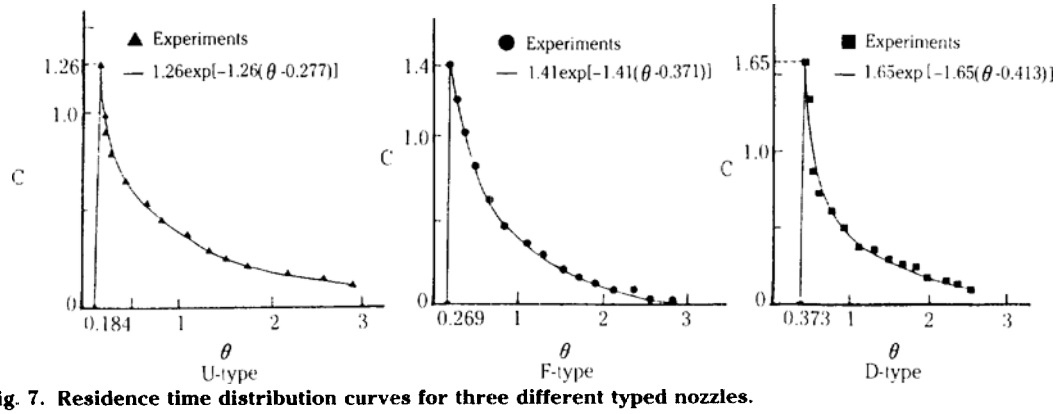

Fig. 7. Residence time distribution curves for three different typed nozzles.

Table 4. Flow and dead volume fractions in the mold.

Nozzle types	Volume fractions		
	mixed flow	plug flow	dead volume
U-type	0.795	0.184	0.021
F-type	0.709	0.269	0.022
D-type	0.592	0.373	0.035

ing polystyrene particles into the submerged nozzle.

The effect of port angle of submerged nozzle on the separation of nonmetallic inclusion was also examined by using three kind of nozzles named U-type (15° upwards), F-type (0°) and D-type (15° downwards). The geometric data of the nozzles are given in Figure 6.

RESULTS AND DISCUSSION

Residence time distribution (RTD)

A solution of concentrated KCl was injected, as quickly as possible, into the water stream immediately under the nozzle and the change of conductivity in the water was measured at the outlet of the mold as a function of time in order to determine the residence time distributions. The RTD's were obtained quite differently for the various types of nozzles.

All the data from the experiments were tested by fitting an appropriate exponential decay curve to the C-diagram and the multiparameter model was found to fit this case as shown in Figure 7. The C-diagrams in the Figure show that the maximum tracer concentration is observed at time $\theta < 1$, this phenomenon indicates the presence of a dead volume in the mold.

The percentages of mixed flow, plug flow and dead volumes were calculated from the RTD curves and presented in Table 4. According to Table 4, U-type nozzle has maximum mixed flow volume and minimum plug flow and dead volumes. In the plug flow, a fluid element moves through the mold without overtaking or mixing with other fluid elements. And dead regions will be subject to decrease the actual average fluid residence time. It serves no purpose in the mold. Therefore, U-type nozzle is most effective for the removal of nonmetallic inclusions in the sense of RTD analysis.

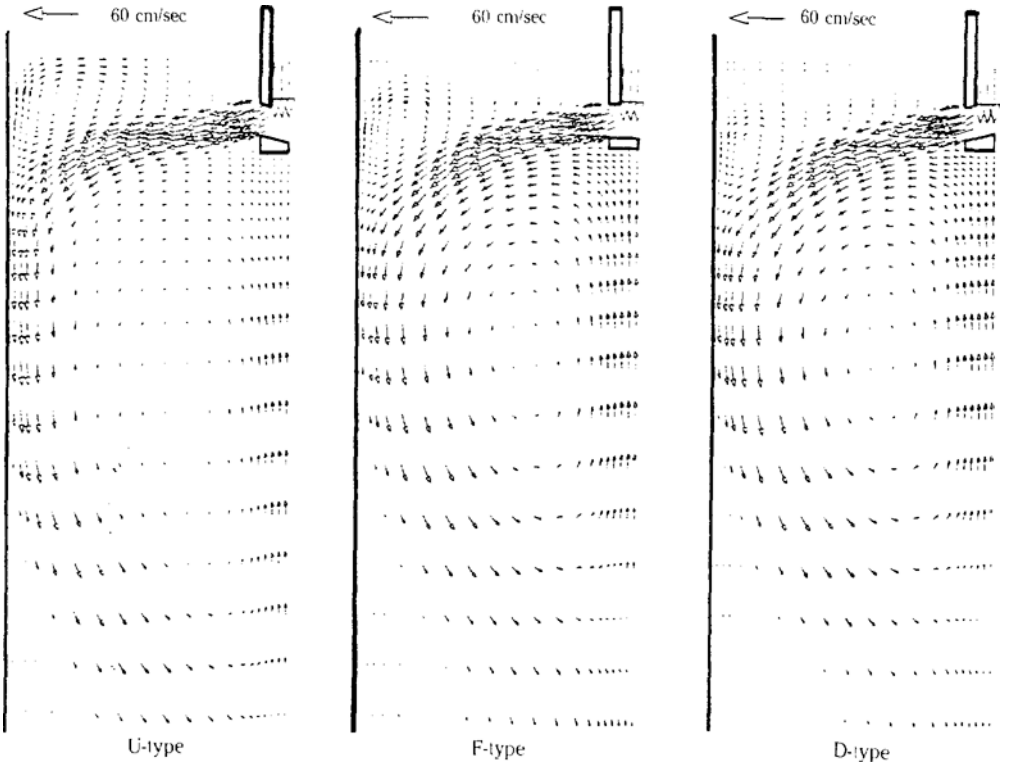

Fig. 8. Predicted velocity fields in the mold.

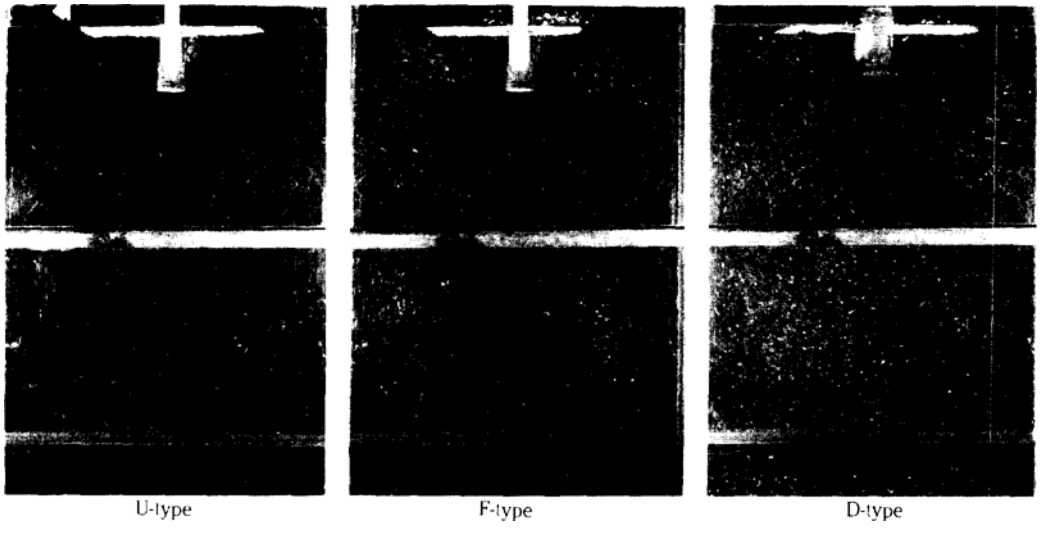

Fig. 9. Observed flow patterns in the mold.

Flow patterns in the mold

Figure 8 shows the computed velocity vectors in the mold when U, F, and D-type nozzles were used. The stream from the nozzle branches off into one upward and one downward flow after hitting the narrow side of the mold. Upward stream turns into the vertical flow along the wall, and the U-type nozzle gives strong upward flow velocities. Vortex regions near the meniscus of the mold are formed by upward streams.

According to Szekely [2], the rising velocity of the

stream is a driving force for floatation. Hereby, inclusions can reach the top surface and be entrapped due to the upward flow. Therefore, it is found that U-type nozzle gives flow patterns that are more conducive to the floatation of inclusions than those appeared by the F- or D-type nozzles. However, the meniscus in the mold with U-type nozzle exhibits a wave motion and consequently the maintenance of mold powder layer on the meniscus of the mold is somewhat difficult.

The observed flow fields in the mold with different nozzles clearly show a recirculating vortex located near the meniscus and the center region of the mold as depicted by Figure 9. From Figures 8 and 9 it can be seen that the numerical predictions of flow patterns are in good qualitative agreement with the experimental results.

In the present study, the flow patterns in the thin casting mold were successfully simulated by using two-dimensional cavity model. However, further extension to general three-dimensional problem could give valuable contributions toward numerical simulations. A generalization of the present study is currently under way in this research group.

CONCLUSION

To study removal of nonmetallic inclusions in a continuous casting mold, both flow visualized experiments and computer simulations were carried out using a 1/2 scale water model of the actual mold. The velocity fields predicted by solving the turbulent Navier-Stokes equations using the K-ε model for turbulent viscosity were found to be in good qualitative agreement with the results of water model experiments.

The effect of port angle of submerged nozzle on the separation of nonmetallic inclusion was also examined. From the results of RTD experiments and flow field analysis, it could be concluded that upward type nozzle is most effective for the removal of nonmetallic inclusions.

NOMENCLATURE

C : dimensionless concentration
C_D : constant defined by equation (8)
C_{max} : maximum concentration
G : a function defined by equation (19)
K : turbulent kinetic energy
L : length of the mold
P : pressure
S_k : a function defined by equation (17)
S_ε : a function defined by equation (18)
T : thickness of the mold
u_i, u_j : tensorial notation of turbulent velocity vector
V : mold volume
V_d : dead volume
V_m : mixed flow volume
V_p : plug flow volume
W : width of the mold
x_i, x_j : tensorial notation of position vector

Greek Letters

ε : turbulent energy dissipation rate
θ : dimensionless time
θ_{av} : average residence time
θ_{peak} : peak time
μ : viscosity
ξ : vorticity
ρ : density
ψ : stream function

REFERENCES

1. Kemeny, F., Harris, D.J., McLean, A., Meadowcroft, T.R. and Young, J.D.: *AIME Proc. Tech. Conf.*, **2,** 232 (1981).
2. Szekely, J. and Yadoya, T.: *Metal. Trans.* (B), **3,** 2673 (1972).
3. Xiu, W.T. and Carlsson, G.: *Scand. J. Metal.*, **12,** 121 (1983).
4. Sahai, Y. and Ahuja, R.: *Iron. Steel.*, **13,** 241 (1986).
5. Levenspiel, O.: "Chemical Reaction Engineering", Wiley and Sons, New York, NY (1972).
6. Szekely, J. and Themelis, N.J.: "Rate Phenomena in Process Metallurgy", Wiley and Sons. New York, NY (1971).
7. Launder, B.E. and Spalding, D.B.: *Comp. Math. Appl. Mech. Eng.*, **3,** 269 (1974).
8. Roache, P.J.: "Computational Fluid Dynamics", Hermosa, Albuquerque, NM (1972).
9. Gosman, A.D., Pun, W.M., Runchal, A.K., Spalding, D.B. and Wolfshtein, M.W.: "Heat and Mass Transfer in Recirculating Flows", Academic Press, London (1969).
10. Johnstone, R.E. and Thring, M.W.: "Pilot Plants, Models and Scale-Up Methods in Chemical Engineering", McGraw-Hill, New York. NY (1957).